Journal of Magnetic Resonance **153,** 203–209 (2001)
doi:10.1006/jmre.2001.2442, available online at http://www.idealibrary.com on IDEAL®

^{1}H Spectroscopy without Solvent Suppression: Characterization of Signal Modulations at Short Echo Times

David B. Clayton,*[,1] Mark A. Elliott,* John S. Leigh,* and Robert E. Lenkinski†

*Department of Radiology, University of Pennsylvania, Philadelphia, Pennsylvania 19104; and †Beth Israel Deaconess Medical Center, Department of Radiology, Harvard Medical School, Boston, Massachusetts 02215

Received March 26, 2001; revised August 30, 2001; published online October 25, 2001

While most proton (^{1}H) spectra acquired *in vivo* utilize selective suppression of the solvent signal for more sensitive detection of signals from the dilute metabolites, recent reports have demonstrated the feasibility and advantages of collecting *in vivo* data without solvent attenuation. When these acquisitions are performed at short echo times, the presence of frequency modulations of the water resonance may become an obstacle to the identification and quantitation of metabolite resonances. The present report addresses the characteristics, origin, and elimination of these sidebands. Sideband amplitudes were measured as a function of delay time between gradient pulse and data collection, as a function of gradient pulse amplitude, and as a function of spatial location of the sample for each of the three orthogonal gradient sets. Acoustic acquisitions were performed to demonstrate the correlation between mechanical vibration resonances and the frequencies of MR sidebands. A mathematical framework is developed and compared with the experimental results. This derivation is based on the theory that these frequency modulations are induced by magnetic field fluctuations generated by the transient oscillations of gradient coils.

Key Words: **unsuppressed; sideband; gradient coil; acoustic vibration.**

INTRODUCTION

The overwhelming majority of proton (^{1}H) spectra acquired *in vivo* utilize selective suppression of the solvent signal to reduce the dynamic range for more sensitive detection of signals arising from the dilute metabolites. Several recent reports have demonstrated the feasibility and advantages of collecting *in vivo* data without solvent suppression (*1–4*). However, a serious impediment to such acquisitions performed at short echo times (TE) is the presence of parasitic frequency modulations of the water resonance (*2, 3*). These spurious modulations, or sidebands, appear as severe baseline distortions in band-limited regions throughout the spectra. They can make accurate quantitation of metabolite signals difficult or impossible. This work addresses the characteristics, origin, and elimination of these sidebands.

[1] Current address: Department of Radiology, Stanford University, Lucas Center for MR Spectroscopy and Imaging, Stanford, CA 94305. E-mail: dclayton@stanford.edu.

In general, it is well known in the field of high-resolution MR that the acquisition of resonances with large signal-to-noise ratios (S/N) reveals spurious artifacts that are the result of instrumentation imperfections (*5*). These artifacts are referred to as cycling sidebands in MAS MR where the high frequency rotation of the sample about the magic angle in an imperfect polarizing field causes the sample to experience periodic time-varying field fluctuations (*6, 7*). In broadband decoupling experiments, similar sidebands arise from field modulations transmitted via spin–spin interactions during periodic sequences of composite pulses (*8, 9*).

In this investigation, it is proposed that the general instrumentation imperfection giving rise to the MR spectral modulation components is the flexibility and motion of the gradient coils that produce magnetic field fluctuations (*10*). Following a gradient pulse, these coils distort and return to equilibrium under damped oscillatory motion. Such coil vibrations produce time-varying fields in the sample that in turn generate sidebands in localized proton spectra. Two methods are presented here to illustrate and characterize this dependence. First, measurement of sound pressure levels (*11*) was employed as a method of detecting the vibration of the gradient coils. These acoustic acquisitions are compared with simultaneously acquired MR spectra. Second, the characteristics of the sidebands appearing in MR spectra were observed as a function of spatial location, gradient strength, and delay time between signal acquisition and gradient pulse.

MATERIALS AND METHODS

All of the proton MR spectra were acquired on a 1-m-bore whole-body 4 T Signa MR scanner (GE Medical Systems, Milwaukee WI) using a standard GE quadrature birdcage head coil to transmit and receive. The gradient set has a maximum strength of 2.2 G/cm with a 184-μs rise time and a 11.96-G/(cm · ms) slew rate. No water suppression was applied during any of the acquisitions.

Localized Spectra

To demonstrate the occurrence of the sidebands in a typical MR experiment, spectra were acquired from a $2 \times 2 \times 2$-cm^3

1090-7807/01 $35.00

voxel in a spherical "head" phantom containing 12.5 mM *N*-acetylaspartate (NAA), 10 mM creatine (Cr), 3 mM choline (Cho), and 5 mM lactate (Lac). PRESS localization was used with several different TE values ranging from 20 to 288 ms. Acquisitions were averaged over 64 excitations (NEX) with a repetition time (TR) of 2 s.

To demonstrate the effect of crusher gradients used during localization, two slice-selective spectra were recorded from the phantom using a spin echo pulse sequence. One spectrum was acquired in typical fashion with two crusher gradients on each of the three gradient axes: one preceding and one following the refocusing pulse. In the second acquisition, all crusher gradients were turned off and a two-step phase cycling scheme was used in which the polarity of the 90° excitation pulse was alternated between successive repetitions with a concomitant reversal in receiver phase. Both were acquired from a 5-mm slice (TE 40 ms, TR 1 s, and 64 NEX).

Sideband Characterization

Unlocalized FID signals (TR 1 s, 64 NEX) were acquired from a 25-mL round-bottom flask containing distilled water. The phantom was placed at 14 different positions inside the magnet, $P(x, y, z)$ where $x, y, z = \pm 10, 0$ cm, as shown in Fig. 1. The position of the head coil relative to isocenter, $P(0, 0, 0)$, was kept constant for all acquisitions and certain locations were physically disallowed by the geometry of the head coil.

At each position, the shim was manually optimized by finding the maximum of the magnitude spectrum. One baseline acquisition was made without any gradient pulses and considered to be the "pure water" signal in that it was free from sideband distortions. Other spectra were acquired with a single gradient pulse on one of the three orthogonal axes (G_x, G_y, G_z) preceding the RF excitation by a delay time, T_d, which was varied from 5 to 200 ms. A diagram of the pulse sequence timing is shown in Fig. 2. The duration of the gradient pulse was 14 ms and its amplitude was varied ±1.76 G/cm. An example of the timing of the acoustic acquisition relative to the NMR excitation is also shown in Fig. 2.

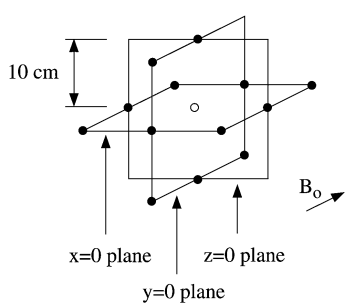

FIG. 1. The locations of the 25 mL water phantom. The center, unfilled circle represents the magnet's isocenter, $P(0, 0, 0)$. The z-axis is parallel to the B_0 field. All orthogonal displacements are 10 cm.

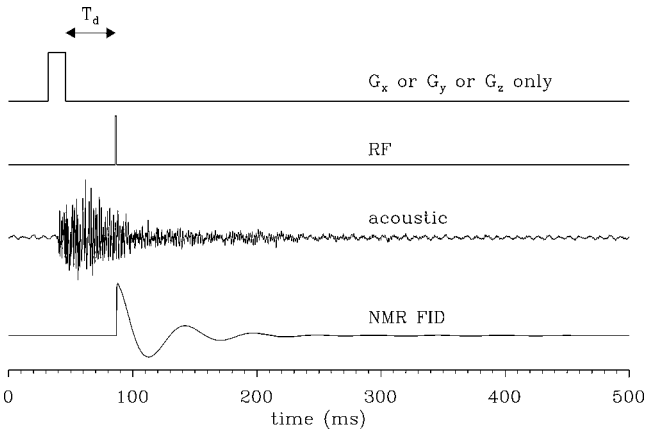

FIG. 2. Timing diagram of a simple pulse–acquire sequence preceded by a single gradient pulse. Also shown are typical raw acoustic and FID signals.

Acoustic Signal Acquisitions

The mechanical vibration of the gradient sets transduced into sound pressure levels was measured by recording the audio signal from the two microphones that are part of the Signa patient intercom system. The signals from the two microphones, one at each end of the magnet bore, were summed and filtered by two 24 dB/octave low pass filters with a −3 dB frequency set at 2 kHz. The signal was sampled at 10 kHz and digitized to 12 bits using a multifunctional interface to a laptop computer. Acquisition of the analog signal (audio input from the microphones) was triggered by a TTL signal generated by the scanner's integrated pulse generator at the beginning of each TR interval. The triggering allowed for 32 signals to be averaged.

RESULTS

Localized Spectra

Figure 3 shows absorption spectra acquired from the head phantom at different TE values using PRESS localization. The approximate locations of modulation sidebands are indicated by the arrows. Figure 4 shows the metabolite region of the two absorption spectra acquired from a slice in the head phantom with and without crusher gradients around the refocusing pulse.

Sideband Characterization

Figure 5 shows the spectra acquired from the 25 mL water phantom at all 14 spatial locations when the gradient pulse is on G_x only. Each absorption spectrum is the result of subtracting the phased pure water spectrum (acquired without G_x pulse) from the phased spectrum containing sidebands (acquired with G_x pulse) for a given sample position. This subtraction was performed to reduce the steep baseline shoulder of the large water signal that extends into the region of the sideband locations. Prior to subtraction, an automated zero-order phase correction and 3 Hz line broadening was applied to both spectra.

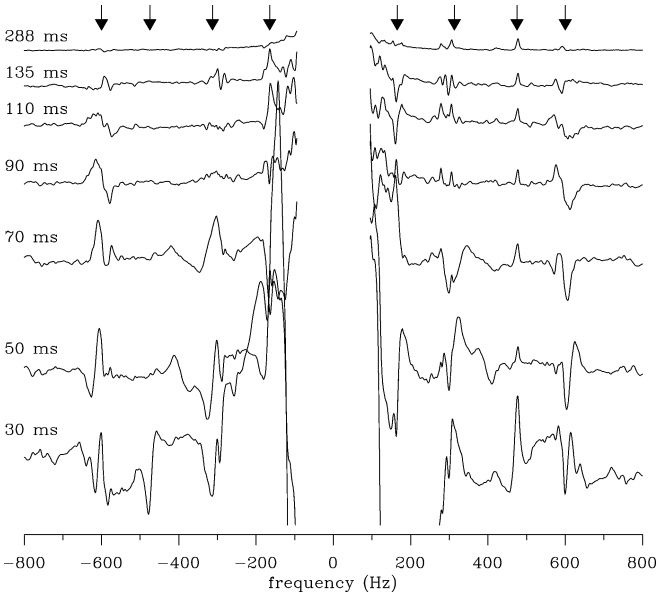

FIG. 3. PRESS acquisitions at various TE values from a single-voxel in the head phantom. Locations of prominent sidebands are indicated by the arrows. TE values are given at the left of each spectrum.

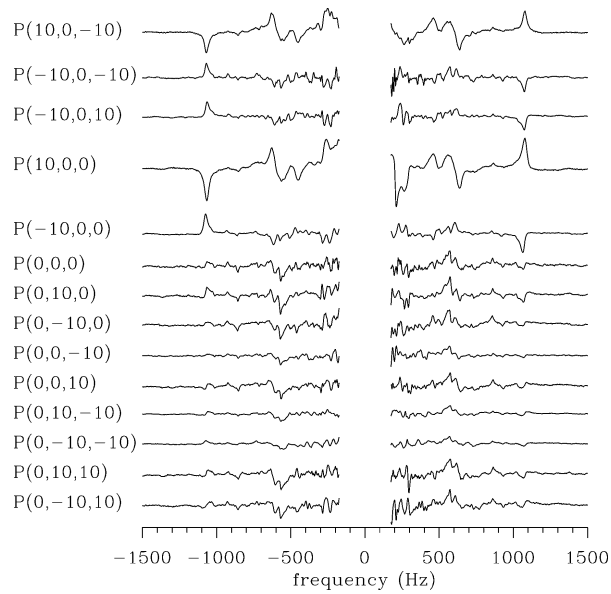

FIG. 5. Spectra from a 25 mL water phantom at 14 different locations (see Fig. 1) with a single gradient pulse on G_x (see Fig. 2). A pure water signal (see text for description) was subtracted from each signal for display. An automated zero-order phase correction was applied to both spectra prior to subtraction and 3-Hz line broadening was applied. The position, $P(x, y, z)$, is indicated at the left. The top five spectra (acquired with the phantom off the $x = 0$ plane) contain significant sidebands at ± 1050 Hz. The other nine spectra (acquired with the phantom on the $x = 0$ plane) do not contain significant sidebands.

Figure 6 shows the absorption spectra at various T_d values, between G_y and the RF pulse. The sample was positioned 10 cm off isocenter in the y direction, $P(0, 10, 0)$, and the gradient strength was 1.67 G/cm. To quantify the decay time of sideband amplitude in the spectra, the moduli of two regions exhibiting prominent sidebands were integrated. Prior to integration, a linear approximation to the water baseline in the region was subtracted. The areas of the two sideband regions were averaged and then normalized by dividing the water amplitude. This normalization step was implemented to compensate for B_1 inhomogeneities of the head coil. A plot of the sideband-to-water ratios as a function of T_d is shown in Fig. 7. A single decaying

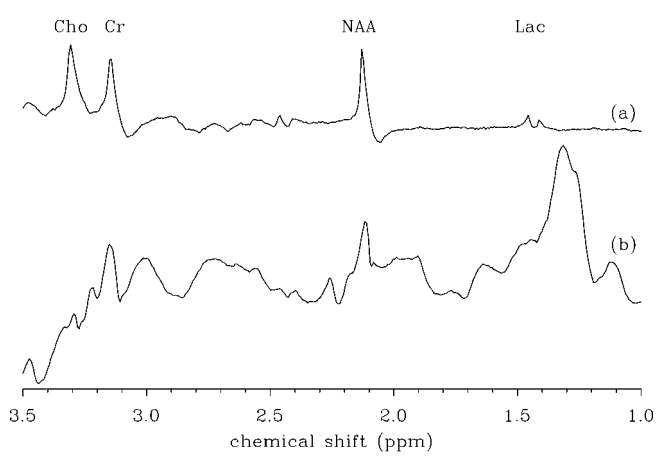

FIG. 4. Spectra acquired with a spin echo sequence from a 5-mm slice in the head phantom (b) with and (a) without crusher gradients.

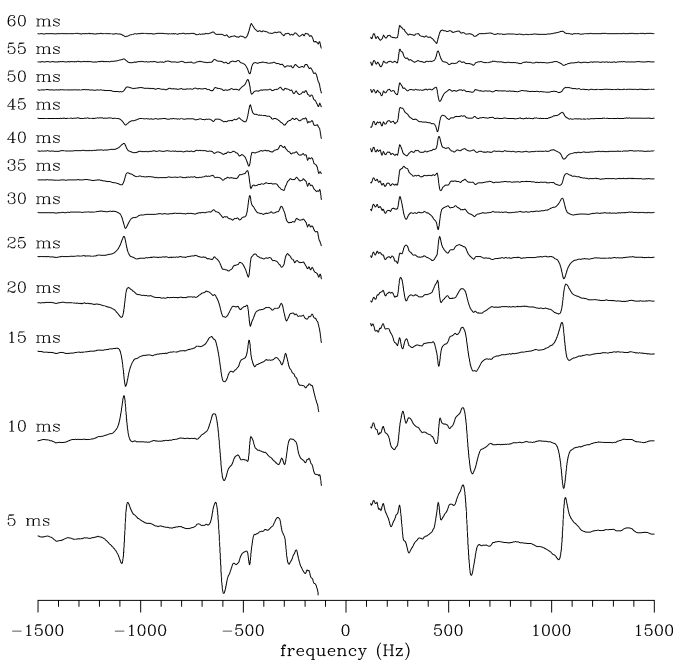

FIG. 6. Spectra acquired from a 25 mL water phantom at $P(0, 10, 0)$ with various values for the delay between gradient pulse and acquisition window, T_d (shown at the left of each spectrum), and with a single gradient pulse on G_y. Spectra were processed for display as described in Fig. 5.

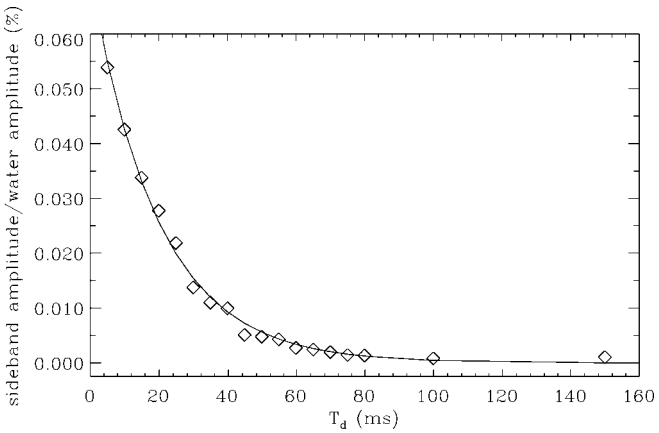

FIG. 7. Plot of the sideband amplitude expressed as a ratio to the water amplitude for G_y as a function of the delay between gradient pulse and acquisition window, T_d. Shown are the experimental values (diamonds) derived from Fig. 6 (see text for explanation) and the best-fit exponential decay curve (solid line).

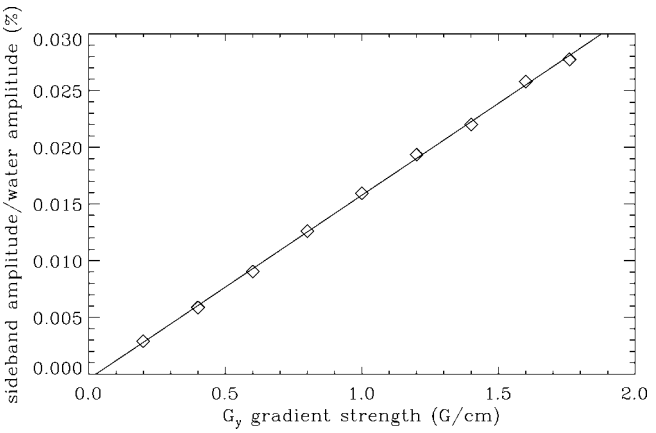

FIG. 9. Plot of the sideband amplitude expressed as a ratio to the water amplitude for G_y as a function of gradient pulse strength. Shown are the experimental values (diamonds) derived from Fig. 8 (see text for explanation) and the linear best-fit (solid line).

exponential model function was used to fit the data (solid line in Fig. 7) and the best estimate of the decay time of the sideband amplitude for G_y was found to be 19.7 ms.

Spectra acquired from $P(0, 10, 0)$ with $T_d = 20$ ms for which the amplitude of G_y was varied from 0.2 to 1.76 G/cm are shown in Fig. 8. Using the same method described above for determining the sideband amplitude, the plot shown in Fig. 9 was made to illustrate the dependence of sideband amplitude on gradient strength which was estimated with a linear model. The best estimate of the slope was determined to be 0.0162% $(\text{G/cm})^{-1}$.

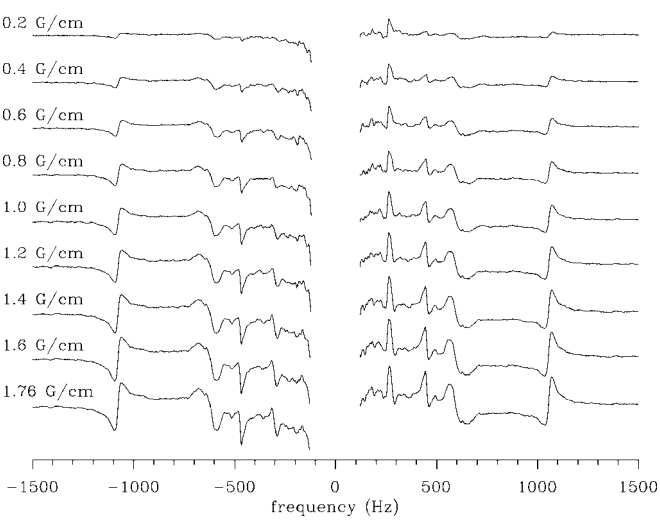

FIG. 8. Spectra acquired from a 25 mL water phantom at $P(0, 10, 0)$ with various values for the gradient pulse amplitude on G_y (shown at the left of each spectrum) and with a fixed T_d of 10 ms. Spectra were processed for display as described in Fig. 5.

Comparison of MR and Acoustic Acquisitions

The acoustic spectra for G_y and G_x are shown in Fig. 10 with the corresponding MR spectra. The S/N for the G_z acoustic signal was too small to determine significant resonances. Arrows are shown to indicate the coincident locations of MR sidebands and acoustic resonances.

DISCUSSION

It is evident from Fig. 3 that sideband distortions occur in localized, unsuppressed spectra and that these distortions increase in magnitude as the TE is shortened. The sidebands occur in pairs equidistant from the water resonance (±175, ±300, ±490, and

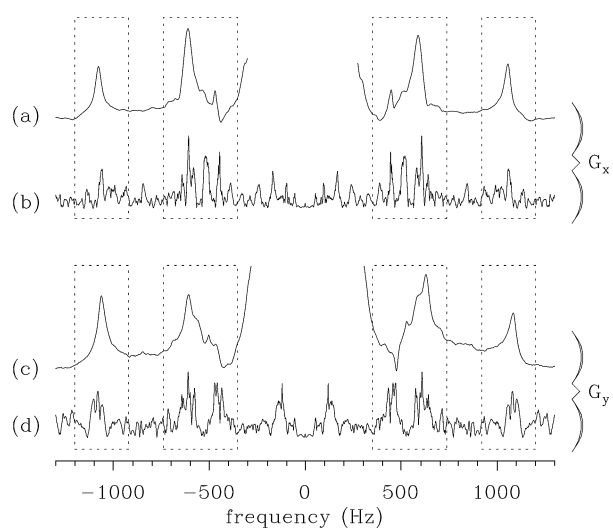

FIG. 10. Acoustic (b and d) and MR (a and c) magnitude spectra acquired with gradient pulses on G_x (a and b) and for G_y (c and d). The dotted boxes indicate the coincident locations of MR sidebands and acoustic resonances.

±600 Hz). The up-field sideband appears approximately 180° out of phase with respect to its down-field partner. Several of these pairs are observed, but are not necessarily evenly spaced. This is because different gradient pulses (slice selective, crushers, etc.) have different timings and excite different gradient coils and may have different resonant responses. For the particular gradient system used in this study, the frequency of one particular sideband coincided with the metabolite region causing considerable distortions. In fact, even for TE values as long as 90 ms, while most metabolite signals are observable, the sidebands significantly disturb the baseline so as to limit the accuracy of quantitation. Similar observations were made with STEAM and spin echo sequences.

Figure 4 shows that by removing the large crusher gradient pulses that occur prior to read-out by a time less than TE/2, it is possible to drastically reduce the interference of modulation resonances. Crusher gradients are typically used to dephase undesirable coherences when phase cycling is not possible (e.g., single NEX experiments). Since it is often desirable or necessary to increase the NEX to improve S/N of *in vivo* spectra, this method of sideband reduction via replacement of crusher gradients with RF phase cycling is quite viable.

The positional spectra from the 25 mL water phantom map the spatial dependence of the three orthogonal gradient axes and the individual contributions of separate gradient axes to the more complex sequences. While data presented here (Fig. 5) was acquired for a G_x pulse only, analogous data were acquired for the two other orthogonal gradient sets, all of which lead to the following observations:

1. Each gradient set contributes negligible sidebands to spectra acquired from that gradient's geometric zero plane. This is demonstrated in Fig. 5 where all spectra on the $x = 0$ plane, $P(0, y, z)$ for any y or z, exhibit negligible sidebands. However, spectra off the $x = 0$ plane, $P(\pm 10, y, z)$ for any y or z, exhibit appreciable sidebands.
2. At positions reflected across a gradient's zero plane, each sideband's phase changes 180°. Compare, for instance, spectra from $P(10, 0, 0)$ to $P(-10, 0, 0)$ and $P(10, 0, -10)$ to $P(-10, 0, -10)$ in Fig. 5.
3. As described above for the PRESS spectra, all sidebands occur in distinct bipolar pairs. In Fig. 5, pairs occur at ±1050 Hz.

The first two observations indicate that there is an antisymmetric oscillatory motion responsible for producing the sidebands and that the plane of reflection is consistent with the structure of the gradient sets (*12*). The third observation is indicative of damped oscillatory motion that will be discussed further in the section on theoretical modeling.

The variation in amplitudes of the sidebands in spectra acquired when the phantom was off the zero plane as well as the appearance of small sidebands when the phantom is on a zero plane are most likely due to inexact placements of the phantom. Also, because the lineshapes of the sidebands depend on the lineshapes of the water resonance (as will be discussed below), distortions in the shapes of the sidebands from position to position are most likely the result of imperfect shimming.

The connections between gradient pulses and sidebands are further demonstrated in Figs. 7 and 9. The former reveals an exponentially damped dependence between sideband amplitudes and the time from gradient pulse to data collection; the latter reveals a linear dependence between the strength of gradient pulses and sideband amplitudes. Both of these conditions are indicative of what is expected if the sidebands are linked to the damped oscillatory behavior of the gradient coil vibrations following an initial disturbance (pulse).

Figure 10 shows good agreement between the frequencies of acoustic resonances and MR sidebands. Since the acoustic signal is assumed to be purely the result of mechanical vibrations of the gradient system, these correlations to the sideband behavior further support the idea that the origin of the sidebands lies in the pulsing of gradients: as switching gradients give rise to sound pressure levels which are detected here through audio medium, they also give rise to time-varying gradient fields which are indirectly detected through MR methods in the form of signal modulations.

The production of the time-varying gradient can be thought of as a two-step process: (1) the initial distortion of the gradient coils and (2) the subsequent oscillatory relaxation. Every time a current is produced in a gradient coil by application of crusher, spoiler, or slice-selection pulse, a Lorentz force is exerted on the coil through the interaction between the B_0 field and the current being conducted through the coil. Following this initial strain, the coil relaxes to its unperturbed state and, while doing so, generates the time-varying field responsible for modulating the MR signal. One suggested means for this field production by the vibrating coil is though the changing B_0 flux which establishes an EMF in the coil. The gradient power supply acts to negate this EMF by injecting current which then creates a time-varying magnetic field in the bore. Another possible mechanism is that the oscillating boundary conditions imposed by the electromagnetic properties of the coil are enough to modulate B_0 itself.

This discussion leads to a comparison between gradient-induced signal modulations and eddy current artifacts (*13*). Both are the result of rapidly switching gradient pulses. But, whereas eddy currents are induced in the magnet cryostat, the fields producing sidebands are generated by the gradient coils themselves. Both phenomena produce time- and spatial-varying magnetic fields in the sample. Eddy currents, however, exhibit critically damped relaxation (*14*), whereas the transient response of the sideband modulations is underdamped via the ring-down of the gradient vibrations.

Furthermore, there is a distinction in amplitude and phase effects. The amplitudes of eddy current artifacts are solely dependent upon the size of the eddy currents produced in the cryostat, whereas the amplitudes of sidebands depend not only on the magnitude of gradient coil displacements, but on the amplitude of the modulated signal as well. The amplitude of sideband

distortions is dependent on the MR signal itself, but the same is not true for eddy current artifacts. The phase distortion in MR signals produced by eddy current effects typically results in asymmetric lineshapes (*15*) of all the resonances in a spectrum. Sideband modulations, however, leave the original signal undisturbed but distribute distortions at regular frequency intervals throughout the spectrum. It is these satellite distortions that may interfere with *other* resonances.

THEORETICAL MODEL AND SIMULATION

It is possible to model the sidebands as a frequency modulation of the MR signal. The FID signal, $s_j(t)$, as a function of time, t, of a single spin isochromat, j, at a localized point in space can be expressed as

$$s_j(t) = A_j e^{-t/T_{2j}} e^{i\omega_j t}, \qquad [1]$$

where $\omega_j = 2\pi f_j$ is the angular resonant frequency, T_{2j} is the relaxation time, A_j is the complex amplitude containing $t = 0$ phase information, and $i \equiv \sqrt{-1}$. The frequency is related to the total effective magnetic field, H_j, by the well-known Larmor relation, $\omega_j = \gamma H_j$, where γ is the gyromagnetic ratio of the nucleus under consideration. The total detected signal, $s(t)$, is the sum over all N isochromats in the excited region of the sample:

$$s(t) = \sum_{j=1}^{N} s_j(t). \qquad [2]$$

Equation [1] assumes that the magnetic field and, hence, the frequencies of all isochromats are independent of time. In a manner analogous to the application of localizing gradient fields, this expression can be revised to include a time-varying field perturbation produced by the oscillating gradient coils. The total field experienced by each isochromat can be considered as the superposition of two terms,

$$H_j \rightarrow H_j + \tilde{H}(t), \qquad [3]$$

where the time-varying field produced by the damped ringing of the gradient coils, $\tilde{H}(t)$, has been separated from all other magnetic fields, H_j. The latter includes terms from the static polarizing field, chemical shift, RF, localization gradients, shimming inhomogeneity, local susceptibility inhomogeneity, etc. Note that $\tilde{H}(t)$, unlike H_j, is independent of the particular isochromat; i.e., it is a term which applies to *all* spins.

Similarly for the resonant frequencies via the Larmor relation,

$$\omega_j \rightarrow \omega_j + \tilde{\omega}(t), \qquad [4]$$

and now Eq. [1] must be written in the following way,

$$\tilde{s}_j(t) = A_j e^{-t/T_{2j}} e^{i\omega_j t} e^{i\theta(t)}, \qquad [5]$$

where

$$\theta(t) = \int_0^t \tilde{\omega}(t')\, dt'. \qquad [6]$$

Because the term involving $\theta(t)$ in Eq. [5] is independent of j (as alluded to at the end of the previous paragraph), it can be brought outside the summation in Eq. [2] and the total modulated signal can be written as

$$\tilde{s}(t) = e^{i\theta(t)} s(t). \qquad [7]$$

This final expression implies that, in theory, every resonance in a spectrum is accompanied by its own set of sidebands, but because the sidebands are such a small fraction of the resonance which produces them (10^{-4} to 10^{-5} times smaller, as found here), metabolites and the residual water in solvent suppressed proton spectra have sidebands that are indistinguishable from noise, even for the largest gradient strengths and shortest T_d (or TE) values.

If the oscillatory motion of the gradient coils is modeled as a damped sinusoid, then the perturbation frequency can be written as

$$\tilde{\omega}(t) = \gamma \tilde{H}(t) = A_m \sin(\omega_m t + \phi_m) e^{-t/T_m}, \qquad [8]$$

where ω_m is the frequency of vibration, T_m is the damping time, A_m is the amplitude, and ϕ_m is an arbitrary phase factor. Simulated spectra were generated using Eqs. [5], [6], and [8] for a single resonance ($N = 1$) and are shown in Fig. 11. There is good agreement between the features of these simulations and those in the experimental results. Furthermore, knowledge of this model function may lead to successful postprocessing techniques for the selective reduction of side amplitudes (*16, 17*).

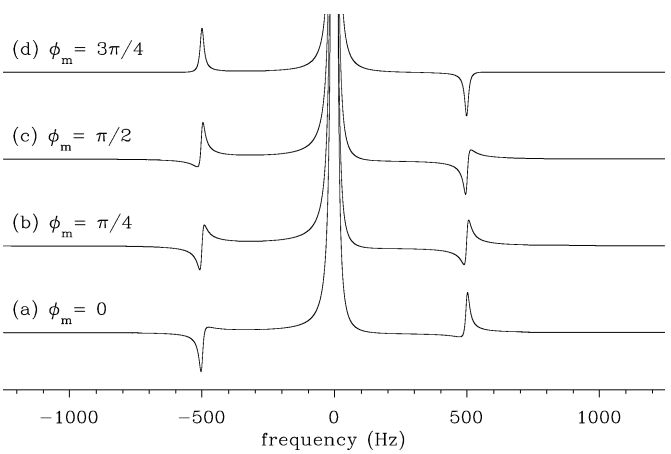

FIG. 11. Simulated spectra with sidebands. Each signal was generated in the time domain using Eqs. [5], [6], and [8] with $N = 1$, $A = 1$, $T_2 = 50$ ms, $\omega = 0$ Hz, $A_m = 100$, $\omega_m = 500/2\pi$, and $T_m = 30$ ms. The arbitrary phase of the perturbation, ϕ_m, was set to 0 in (a), $\pi/4$ in (b), $\pi/2$ in (c), and $3\pi/4$ in (d).

CONCLUSIONS

Parasitic sideband signals are observed in ^{1}H MR spectra that are acquired without solvent suppression and when there is a short delay between large gradient pulses and the acquisition window (in particular, localized short TE experiments). It is proposed that these sidebands are the result of a frequency modulation of the water signal due to oscillating magnetic fields and that these time-varying fields are induced by the mechanical vibrations of gradient coils subsequent to initial distortions which are forced by the current pulses required to produce gradient waveforms. This hypothesis is supported by several observations: (1) sideband characteristics as a function of spatial position, (2) the dependence of sideband amplitude on both the gradient amplitude and delay to read-out, (3) the correlation between the frequencies of acoustic resonances and the sidebands, and (4) the agreement between experimental features and the proposed mathematical model.

ACKNOWLEDGMENTS

This study was sponsored by NIH Grants RR02305, R01-CA70362, R01-MH49390, and R01-NS31464.

REFERENCES

1. D. B. Clayton, M. A. Elliott, and R. E. Lenkinski, *In vivo* proton spectroscopy without solvent suppression, *Concepts Magn. Reson.* **13,** 260–275 (2001).
2. R. E. Hurd, D. Gurr, and N. Sailasuta, Proton spectroscopy without water suppression: The oversampled *J*-resolved experiment, *Magn. Reson. Med.* **40,** 343–347 (1998).
3. D. B. Clayton, M. A. Elliott, and R. E. Lenkinski, *In vivo* proton MRS of the human brain at 4 T without solvent suppression, *in* "Proceedings of the 7th ISMRM Meeting, Philadelphia," p. 1602, 1999.
4. J. W. C. van der Veen, D. R. Weinberger, G. Tedeschi, J. A. Frank, and J. H. Duyn, Proton MR spectroscopic imaging without water suppression, *Radiology* **217,** 296–300 (2000).
5. S. R. Maple and A. Allerhand, Analysis of minor components by ultrahigh resolution NMR. I. Evidence for the detectability of weak resonances near peaks which are 10,000 times larger, without suppression of the large peaks, *J. Magn. Reson.* **72,** 203–210 (1987).
6. L. Marinelli and L. Frydman, On the origin of spinning sidebands in MQMAS NMR experiments, *Chem. Phys. Lett.* **275,** 188–198 (1997).
7. M. W. Borer and S. R. Maple, Control of spinning sidebands in high resolution NMR spectroscopy, *J. Magn. Reson.* **131,** 177–183 (1998).
8. A. J. Shaka, P. B. Barker, C. J. Bauer, and R. Freeman, Cycling sidebands in broadband decoupling, *J. Magn. Reson.* **67,** 396–401 (1986).
9. R. Freeman and E. Kupce, Decoupling: Theory and practice. I. Current methods and recent concepts, *NMR Biomed.* **10,** 372–380 (1997).
10. Y. Wu, B. A. Chronik, C. Bowen, C. K. Mechefske, and B. K. Rutt, Gradient-induced acoustic and magnetic field fluctuations in a 4 T whole-body MR imager, *Magn. Reson. Med.* **44,** 532–536 (2000).
11. R. A. Hedeen and W. A. Edelstein, Characterization and prediction of gradient acoustic noise in MR imagers, *Magn. Reson. Med.* **37,** 7–10 (1997).
12. S. R. Thomas, Magnets and gradient coils: Types and characteristics, *in* "The Physics of MRI" (M. J. Bronskill and P. Sprawls, Eds.), pp. 56–97, American Institute of Physics, Woodbury, NY (1993).
13. L. N. Ryner, P. Stroman, T. Wessel, D. I. Hoult, and J. K. Saunders, Effect of oscillatory currents on MR spectroscopy, *in* "Proceedings of the 6th ISMRM Meeting, Sydney," p. 1903, 1998.
14. C. B. Ahn and Z. H. Cho, Analysis of eddy currents in nuclear magnetic resonance imaging, *Magn. Reson. Med.* **17,** 149–163 (1991).
15. J. R. Roebuck, D. O. Hearshen, M. O'Donnell, and T. Raidy, Correction of phase effects produced by eddy currents in solvent suppressed ^{1}H CSI, *Magn. Reson. Med.* **30,** 227–282 (1993).
16. M. A. Elliott, D. B. Clayton, and R. E. Lenkinski, ^{1}H spectroscopy without water suppression: Removal of sideband modulations at short TE, *in* "Proceedings of the 9th ISMRM Meeting, Glasgow," p. 1667 (2001).
17. H. Serrai, D. B. Clayton, L. Senhadji, C. Zuo, and R. E. Lenkinski, Removal of gradient induced frequency modulations in localized proton spectroscopy, *in* "Proceedings of the 9th ISMRM Meeting, Glasgow," p. 1688 (2001).